

**Nascent state distributions of NO ( $X\ 2\ \Pi$ ) generated from the reaction of S ( $1\ D$ ) with N  $2\ O$  : Intramolecular vibrational-energy redistribution in the reaction intermediate**

Hiroshi Akagi, Yo Fujimura, and Okitsugu Kajimoto

Citation: *The Journal of Chemical Physics* **110**, 7264 (1999); doi: 10.1063/1.478629

View online: <http://dx.doi.org/10.1063/1.478629>

View Table of Contents: <http://scitation.aip.org/content/aip/journal/jcp/110/15?ver=pdfcov>

Published by the [AIP Publishing](#)

---

**Articles you may be interested in**

Correlated *ab initio* investigations on the intermolecular and intramolecular potential energy surfaces in the ground electronic state of the  $O\ 2 - (X\ \Pi\ g\ 2) - HF (X\ \Sigma + 1)$  complex

*J. Chem. Phys.* **138**, 014304 (2013); 10.1063/1.4772653

Nanosecond time-resolved IR emission from molecules excited in a supersonic jet: Intramolecular dynamics of N  $O\ 2$  near dissociation

*J. Chem. Phys.* **123**, 154306 (2005); 10.1063/1.2049271

Exit interaction effect on nascent product state distribution of  $O (1\ D) + N\ 2\ O \rightarrow NO + NO$

*J. Chem. Phys.* **120**, 6430 (2004); 10.1063/1.1649721

*Ab initio* and quasiclassical trajectory study of the  $N (2\ D) + NO (X\ 2\ \Pi) \rightarrow O (1\ D) + N\ 2 (X\ 1\ \Sigma\ g +)$  reaction on the lowest  $1\ A'$  potential energy surface

*J. Chem. Phys.* **113**, 10983 (2000); 10.1063/1.1327263

Nascent rotational and vibrational state distributions of  $NH (X\ 3\ \Sigma -)$  and  $ND (X\ 3\ \Sigma -)$  produced in the reactions of  $N (2\ 2\ D)$  with  $H\ 2$  and  $D\ 2$

*J. Chem. Phys.* **106**, 4985 (1997); 10.1063/1.473546

---



# Nascent state distributions of $\text{NO}(X^2\Pi)$ generated from the reaction of $\text{S}(^1D)$ with $\text{N}_2\text{O}$ : Intramolecular vibrational-energy redistribution in the reaction intermediate

Hiroshi Akagi, Yo Fujimura, and Okitsugu Kajimoto<sup>a)</sup>

Department of Chemistry, Graduate School of Science, Kyoto University, Kitashirakawa-Oiwakecho, Sakyo-ku, Kyoto 606-8502, Japan

(Received 21 December 1998; accepted 21 January 1999)

The nascent internal state distribution of  $\text{NO}(X^2\Pi)$  generated from the reaction,  $\text{S}(^1D) + \text{N}_2\text{O} \rightarrow \text{NO} + \text{NS}$ , has been determined by utilizing the laser-induced fluorescence (LIF) technique. The average vibrational energy of NO relative to the statistically expected value is found to be 37%. This amount is obviously smaller than that of the fragment  $\text{N}^{16}\text{O}$  of the isovalent reaction  $^{18}\text{O}(^1D) + \text{N}_2^{16}\text{O} \rightarrow \text{N}^{18}\text{O} + \text{N}^{16}\text{O}$ , though it is still larger than that of  $^{18}\text{OH}$  produced from the  $^{16}\text{O}(^1D) + \text{H}_2^{18}\text{O}$  reaction. To interpret the observed difference in the product energy partitioning, we have applied the quantal intramolecular vibrational-energy redistribution (IVR) representation to the energy mixing in the collision complex. Using a local-mode vibration model with momentum couplings, we have extracted the crucial factors determining the energy partitioning in these reactions. The reaction system consisting of only heavy mass atoms generally has a large vibrational coupling and a large density of states, both of which favor the rapid energy mixing during the short-lifetime of the intermediate complex. © 1999 American Institute of Physics.

[S0021-9606(99)01715-8]

## I. INTRODUCTION

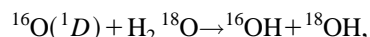
Since the 1970s, the product energy distribution has been a hot topic in reaction dynamics. In particular, the relation between the shape of the potential-energy surface (PES) and the energy partitioning within the degrees of freedom of product molecules has been intensively studied to obtain a fundamental understanding of the dynamics.<sup>1</sup> General criteria for predicting the product energy distribution have been proposed and the analyses using the criteria have attained a marked success.<sup>2</sup> The criteria mainly concern the lifetime of the collision complex or intermediate. As the lifetime becomes longer, the product distribution becomes more statistical. The lifetime of the complex is in turn determined by the shape of the PES. If the potential-energy surface has a deep well between the entrance and the exit, we expect a long lifetime which produces a statistical distribution. On the other hand, if the potential well is much shallower comparing with the exothermicity of the reaction, a short lifetime and a nonstatistical energy partitioning are expected.

In our previous work,<sup>3</sup> we determined the vibrational state distributions of the “new”  $\text{N}^{18}\text{O}$  and the “old”  $\text{N}^{16}\text{O}$  generated from the reaction,



which has a large exothermicity [ $\Delta H^0(0) = -343 \text{ kJ mol}^{-1}$ ] and a shallow well with the N–N bond scission energy of  $\sim 700 \text{ cm}^{-1}$ .<sup>4</sup> Although the available energy is dominantly distributed to the new  $\text{N}^{18}\text{O}$ , the old  $\text{N}^{16}\text{O}$  also possesses a considerable vibrational energy at high vibrational levels. This fact suggests that the considerable energy randomization in the reaction intermediate,  $^{18}\text{ONN}^{16}\text{O}$ , oc-

curs, even though the lifetime of the intermediate complex is expected to be short because of the shallow well of the PES. This efficient energy mixing could be attributed to the constituent atoms in the reaction system, that is, the absence of light atoms. Because the  $^{18}\text{O}(^1D) + \text{N}_2^{16}\text{O}$  system only includes heavy atoms, the energy randomization in the transient  $^{18}\text{ONN}^{16}\text{O}$  should be enhanced due to the large momentum ( $G$ -matrix) couplings between the local-mode vibrations. In addition, the low vibrational frequencies originated from the motion of heavy atoms considerably increase the density of these states. The importance of such mass effect is supported by the inefficient energy mixing between the two OH products observed in the analogous reaction including light H atoms,



$$\Delta H^0(0) = -120 \text{ kJ mol}^{-1}. \quad (\text{b})$$

Since the reaction (b) possesses a deep well, the intermediate of this reaction should have a longer lifetime than that of the reaction (a). Nevertheless, the energy mixing is less efficient in the reaction (b). This evidence suggests the importance of the mass effect over the lifetime of the intermediate complex in contrast to the expectation in general.

In the present study, we try to confirm the critical role of the mass effect by demonstrating another example of efficient energy mixing for the reaction with a short-lived intermediate, i.e.,



Since  $\text{S}(^1D)$  atom is isovalent to  $\text{O}(^1D)$ , this reaction is expected to have a similar PES with no barrier and a very shallow well. In fact, the density functional theory calculations have showed that  $\text{SNNO}$  is a *cis*-planer molecule and

<sup>a)</sup> Author to whom correspondence should be addressed.

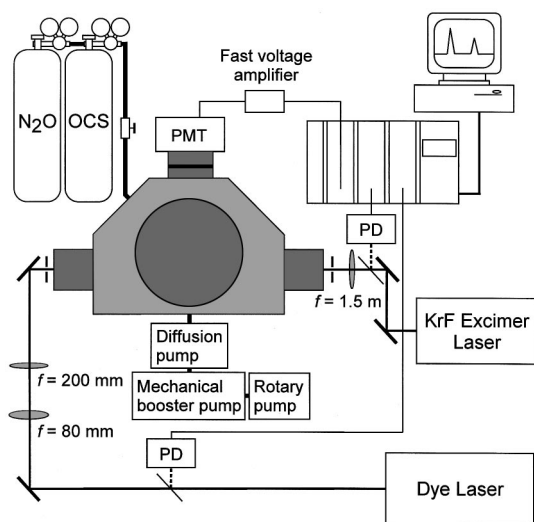
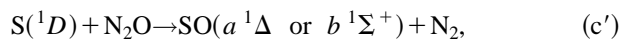


FIG. 1. Schematic diagram of the experimental apparatus. PD, photodiode; PMT, photomultiplier tube.

has a low frequency N–N stretching vibration similar to  $(\text{NO})_2$ .<sup>5</sup> Moreover, this reaction system is composed of four heavy atoms.

The reaction of  $S(^1D)$  with  $\text{N}_2\text{O}$  has been studied by several groups.<sup>6,7</sup> The reaction rate was found to be nearly gas kinetic ( $1.6 \times 10^{-10} \text{ cm}^3 \text{ molecule}^{-1} \text{ s}^{-1}$ ).<sup>6</sup> The reaction has the following two important channels other than channel (c):



These three channels proceed to a comparable extent, although the  $S(^1D)$  quenching process (c'') is slightly preferred.<sup>7</sup>

In the present work, we have dealt with the internal state distribution of  $\text{NO}(X^2\Pi)$  produced from the reaction (c). Because the  $\text{NO}$  molecule is the ‘‘old’’ fragment already existed in the  $\text{N}_2\text{O}$  molecule, the amount of  $\text{NO}$  internal energy is an appropriate index of energy randomization within the reaction intermediate,  $\text{SNNO}$ . The exothermicity of this reaction (c) [ $\Delta H^0(0) \approx -100 \text{ kJ mol}^{-1}$ ] (Ref. 8) can excite the  $\text{NO}$  molecule up to the  $v=4$  vibrational level. We have determined the vibrational ( $v=0-4$ ) and rotational ( $v=0-2$ ) state distributions of  $\text{NO}$  generated by this reaction utilizing the laser-induced fluorescence (LIF) technique.

The quantitative interpretation of the mass effect is also attempted in terms of the intramolecular vibrational-energy redistribution (IVR) in the transient intermediate. The IVR rate is estimated on the basis of the Fermi’s Golden Rule. The state density and the coupling among the vibrational modes are calculated by using the local-mode approximation with the first-order momentum coupling. The quantal time evolution is also calculated to evaluate the rate of IVR.

## II. EXPERIMENT

The experiment was performed with a conventional flow chamber and two laser systems, as shown in Fig. 1. The 1:1

mixture of  $\text{OCS}$  and  $\text{N}_2\text{O}$  gases was continuously supplied to the chamber at 200 mTorr.  $\text{OCS}$  (Matheson 97.5%) and  $\text{N}_2\text{O}$  (Showa-Denko 99.999%) gases were purchased and used without further purification.

The  $S(^1D)$  atoms were produced by  $\text{OCS}$  photolysis at 248 nm with a KrF Excimer laser (Lambda Physik EMG53MSC). The KrF laser light was collected with a lens of 1.5 m focal length, and a part of the focused light ( $\sim 0.5$  cm diam) was used for the photolysis. At this wavelength of  $\text{OCS}$  photolysis, the quantum yield of  $S(^1D)$  generation was already determined to be almost a unity from two photon LIF experiments.<sup>9</sup> The product  $\text{NO}$  generated from reaction (c) was detected by utilizing the LIF technique via the  $\text{NO } A^2\Sigma^+ (v=0,1) \leftarrow X^2\Pi (v=0-4)$  transitions. For this purpose, frequency doubled light from a tunable dye laser (Lambda Physik ScanMate 2E) pumped by a XeCl excimer laser (Lambda Physik Compex 102) was used. In order to avoid saturation, the probe laser light was expanded 2.5 times by two lenses of 8 and 20 cm focal lengths. The intensities of both the photolysis and the probe laser lights were monitored by photodiodes and used to normalize the LIF signal. The time delay between the photolysis and the probe lasers was set to be 500 ns and 5  $\mu\text{s}$  for the determination of rotational and vibrational state distributions, respectively. These laser systems were operated with a repetition rate of 10 Hz.

The fluorescence from  $\text{NO}(A)$  was collected by two lenses at right angles to the counterpropagating laser beams and the fluorescence of only  $(0 \rightarrow 0)$  and  $(1 \rightarrow 1)$  transitions was detected by a photomultiplier tube (Hamamatsu R928) through an interference bandpass filter (the center wavelength  $\lambda_0 = 219.5$  nm, the full bandwidth at half-maximum  $\Delta\lambda = 12.5$  nm). The LIF signal from the PMT was amplified by a fast voltage amplifier (Comlinear CLC100), averaged by a gated boxcar integrator (Stanford Research Systems SR 250), processed by an A/D converter (Stanford Research Systems SR 245), and stored in a personal computer.

For the determination of the vibrational state distribution of  $\text{NO}$  generated from the reaction of  $S(^1D)$  with  $\text{N}_2\text{O}$ , we adopted the same procedure as Ref. 3. Briefly, the procedure consisted of the following two measurements: (1) determination of the rotational state distribution for each vibrational levels under the rotationally relaxed conditions with 200 mTorr total pressure and a 5  $\mu\text{s}$  delay and (2) determination of the relative vibrational population by comparing the peak heights at the selected rotational lines of different vibrational levels. To obtain reliable distribution, we utilized the rovibronic transitions with the same upper levels.

It should be noted that the KrF laser light (248 nm) used for the  $\text{OCS}$  photolysis could also photolyze  $\text{N}_2\text{O}$  and produce  $\text{O}(^1D)$  atoms, even though the absorption coefficient of  $\text{N}_2\text{O}$  at 248 nm is negligibly small.<sup>10,11</sup> The  $\text{O}(^1D)$  atoms, if produced, could also produce  $\text{NO}$  by reaction (a). In fact, the LIF signal from  $\text{NO}$  molecules was detected without the presence of  $\text{OCS}$ . However, for  $\text{NO}$  in  $v=0-3$  and  $v=4$  vibrational levels, the LIF signal in the absence of  $\text{OCS}$  was less than 3% of that with  $\text{OCS}$  and less than the noise level, respectively. Consequently, the contribution from the  $\text{N}_2\text{O}$  photolysis at 248 nm was neglected.

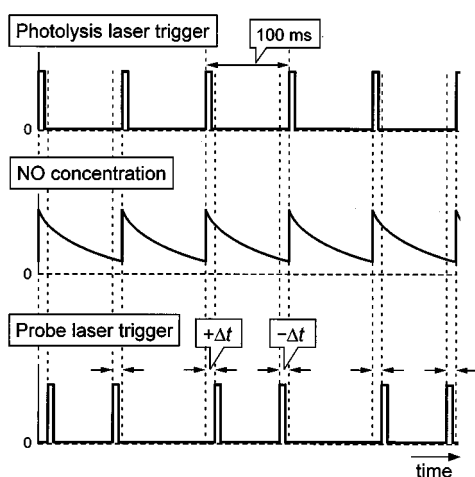


FIG. 2. Schematic diagram of the timing between the two laser triggers and the variation of NO concentration in the reaction cell. Nascent NO ( $v=0$ ) signal was obtained as the difference between the signals of  $\pm\Delta t$  delays in successive laser shots.

A mechanical booster pump and a rotary pump were used for the flowing gas experiment. Since all NO molecules in the  $v=0$  level could not be pumped out perfectly during the shot-to-shot period under the pumping conditions, the LIF signal from NO( $v=0$ ) was detected even when the probe laser light irradiates the reacting gas 500 ns earlier than the photolysis laser light. To determine the nascent signal intensity of NO in  $v=0$  level, the delay time between the photolysis and the probe laser shots was changed alternatively by a homemade switching delay circuit. The signal intensity obtained at  $-\Delta t$  delay corresponds to the background NO( $v=0$ ) signal, and its intensity was subtracted from that obtained at  $+\Delta t$  delay. The timing of such procedure is shown schematically in Fig. 2. Utilizing the subtraction between the two data sets,  $\pm\Delta t$  delays, we obtained accurate LIF spectra of nascent NO molecules.

### III. RESULTS

Figure 3 shows the LIF spectra of the nascent NO( $v=0,1$ ) which is calculated by the subtraction between the two spectra under  $\pm 500$  ns delay conditions, together with the original spectra at each delay. The rotationally relaxed LIF spectrum of NO( $v=3$ ) under 5  $\mu\text{s}$  delay condition is shown in Fig. 4. The simulated spectrum is also included in each of the figures.

As the source of  $S(^1D)$ , we used OCS photolysis at 248 nm. Since  $S(^1D)$  is removed by the every collision with the buffer gas, OCS or  $\text{N}_2\text{O}$ ,<sup>6</sup> the  $S(^1D)$  atom is not translationally relaxed and therefore we should take the collision energy into account. Then, adding the 13  $\text{kJ mol}^{-1}$  collision energy<sup>12</sup> to the heat of reaction, we have the total available energy of 113  $\text{kJ mol}^{-1}$  which could excite the product NO molecule to the  $v=5$  level. In the present experiments, however, we detected the NO up to  $v=4$  vibrational levels under 5  $\mu\text{s}$  delay condition. For  $v=0-2$  vibrational levels, the LIF signal intensity was sufficient to determine the nascent rotational state distribution of NO molecules under the shorter (500 ns) delay condition.

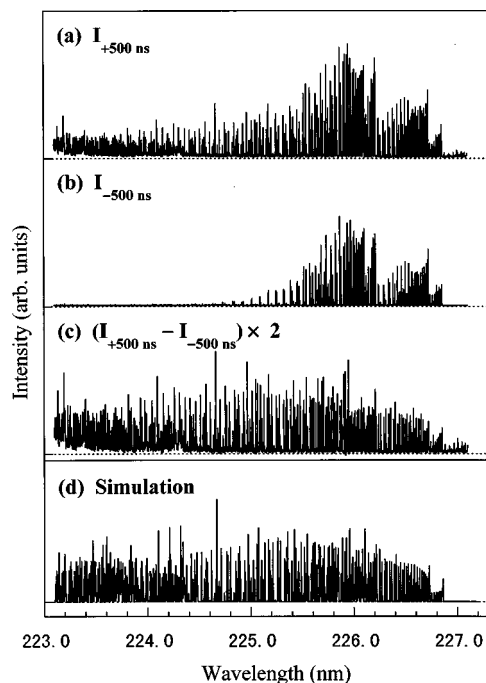


FIG. 3. LIF spectra of NO( $X^2\Pi; v=0$  and 1) generated from the reaction of  $S(^1D)$  with  $\text{N}_2\text{O}$ , together with the simulated spectrum.  $A\leftarrow X(0\leftarrow 0)$  and  $A\leftarrow X(1\leftarrow 1)$  transitions were used. (a) The sum of nascent and background NO signals measured at +500 ns delay. (b) Background NO signal measured at -500 ns delay. (c) Nascent NO signal obtained by taking the difference between signals of  $\pm 500$  ns delays. (d) A spectrum simulated under the conditions of the ratio  $N(v=1)/N(v=0)=0.25$ , and the rotational temperatures 2600 and 1400 K for  $v=0$  and 1, respectively.

### A. Vibrational state distribution in $v=0-4$

The experimentally obtained vibrational state distribution and the distributions predicted from two statistical theories, the prior distribution<sup>1</sup> and the distribution calculated with phase space theory (PST),<sup>13</sup> are listed in Table I. The experimentally obtained population monotonically declines as the vibrational quantum number increases. The observed distribution is slightly colder than those predicted from the

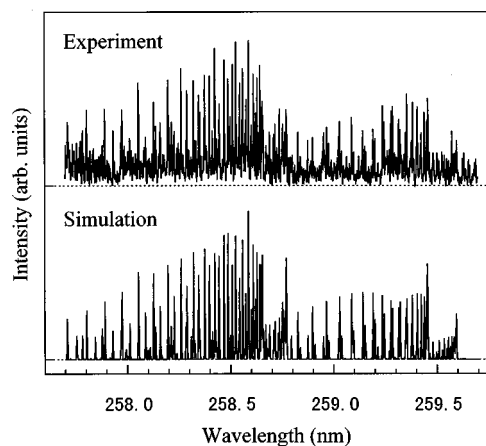


FIG. 4. Rotationally relaxed LIF spectrum of NO ( $v=3$ ) generated from the reaction of  $S(^1D)$  with  $\text{N}_2\text{O}$  utilizing the  $A\leftarrow X(0\leftarrow 3)$  transition (upper panel), together with the simulated spectrum (lower panel). Spectrum taken under 5  $\mu\text{s}$  delay and 200 mTorr total pressure. Simulated spectrum was calculated with a rotational temperature of 320 K.

TABLE I. Vibrational state distribution of NO( $X^2\Pi$ ) generated from the reaction of  $S(^1D)$  with  $N_2O$ .

$v$	Expt <sup>a</sup>	Prior (RRHO)	PST <sup>b</sup>
0	0.76	0.59	0.50
1	0.19±0.04	0.27	0.29
2	0.033±0.008	0.10	0.14
3	0.011±0.003	0.027	0.055
4	0.0004±0.0001	0.003 2	0.012
5	...	0.000 006 3	0.000 18

<sup>a</sup>The experimental uncertainty corresponding to  $1\sigma$  in the least-squares fit.  
<sup>b</sup>For the PST calculation, the interaction potential for both S– $N_2O$  and SN–NO is assumed to have the form of  $-C/r^6$ , where  $C$  is taken to be  $42 \text{ kJ } \text{Å}^6 \text{ mol}^{-1}$ .

statistical theories, as recognized from Fig. 5, suggesting the incomplete vibrational energy randomization in the intermediate. Nevertheless, the “old” NO populate even in  $v=4$  which is the upper limit for the exothermicity of this reaction. This fact indicates that the considerable energy mixing occurs during the reaction.

## B. Nascent rotational state distribution in $v=0-2$

The rotational state distributions for each vibrational level in  $v=0-2$  could be described by a single Boltzmann temperature. The average rotational energy for each vibrational level  $\langle E_{\text{rot}} \rangle_v$  was calculated by the equation

$$\langle E_{\text{rot}} \rangle_v = \sum_J P_v(J) \cdot E_{\text{rot}}(J) / \sum_J P_v(J), \quad (1)$$

where  $P_v(J)$  is the rotational state distribution including the degeneracy and  $E_{\text{rot}}(J)$  is the energy of the rotational state. The evaluated average rotational energies of NO are listed in Table II, together with those predicted from PST.<sup>13</sup> The average rotational energy decreases as the vibrational quantum number increases similar to the statistical prediction. This trend may attribute to the decrease of the available energy. The experimental  $\langle E_{\text{rot}} \rangle_v$  of NO ( $v=0-2$ ) is colder than the average energy expected from PST, yet it is still rotationally excited as compared with the energy at room temperature

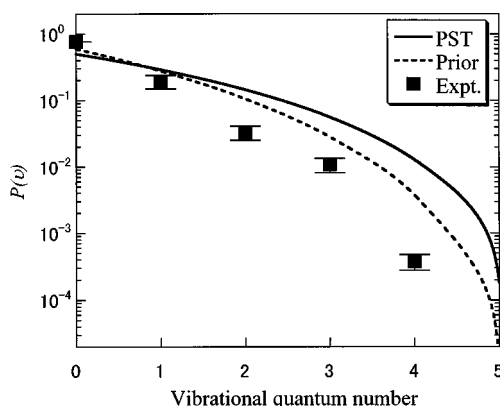


FIG. 5. Vibrational state distribution of NO( $X^2\Pi$ ;  $v=0-4$ ) produced from the reaction of  $S(^1D)$  with  $N_2O$ . The solid line shows the distribution predicted from phase space theory and the broken line depicts the prior distribution.

TABLE II. Average rotational energy  $\langle E_{\text{rot}} \rangle_v$  of NO( $X^2\Pi$ ;  $v=0-2$ ) generated from the reaction of  $S(^1D)$  with  $N_2O$ .

$v$	$\langle E_{\text{rot}} \rangle_v / \text{kJ mol}^{-1}$	
	Expt <sup>a</sup>	PST <sup>b</sup>
0	21.8±0.9	26.0
1	11.3±1.1	21.3
2	9.9±0.4	16.6

<sup>a</sup>The experimental uncertainty corresponding to  $1\sigma$  in the least-squares fit.  
<sup>b</sup>For the PST calculation, the interaction potential for both S– $N_2O$  and SN–NO is assumed to have the form of  $-C/r^6$ , where  $C$  is taken to be  $42 \text{ kJ } \text{Å}^6 \text{ mol}^{-1}$ .

( $2.5 \text{ kJ mol}^{-1}$ ). The latter fact in  $\langle E_{\text{rot}} \rangle_v$  implies that the old NO would not behave simply as a spectator in the  $S(^1D) + N_2O$  reaction.

## C. Energy partitioning to the “old” fragments

The mean rotational and vibrational energies of NO were calculated as

$$\langle E_{\text{rot}} \rangle = \sum_v P(v) \cdot \langle E_{\text{rot}} \rangle_v / \sum_v P(v) \quad (2)$$

and

$$\langle E_{\text{vib}} \rangle = \sum_v P(v) \cdot E_{\text{vib}}(v) / \sum_v P(v), \quad (3)$$

respectively. In these equations,  $P(v)$  is the vibrational state distribution and  $E_{\text{vib}}(v)$  is the energy of each vibrational state. To determine the  $\langle E_{\text{rot}} \rangle$ , we used the  $\langle E_{\text{rot}} \rangle_v$  values for only  $v=0-2$  vibrational levels, since the  $\langle E_{\text{rot}} \rangle_v$  values for  $v>2$  could not be determined. However, this omission has little influence on the accuracy because of the minor population in higher vibrational levels.

The average rotational and vibrational energies of the old NO molecules can act as appropriate measures of the energy randomization in the reaction intermediate. The average energies are calculated to be  $\langle E_{\text{rot}} \rangle = 1600 \text{ cm}^{-1}$  and  $\langle E_{\text{vib}} \rangle = 550 \text{ cm}^{-1}$ , which correspond to 17% and 5.8% of the available energy  $E_{\text{avail}} (\approx 113 \text{ kJ mol}^{-1})$ , respectively. Since the PST calculations predict large values ( $\langle E_{\text{rot}} \rangle_{\text{PST}} = 1900 \text{ cm}^{-1}$  and  $\langle E_{\text{vib}} \rangle_{\text{PST}} = 1500 \text{ cm}^{-1}$ ), we can conclude that the energy randomization in the intermediate of this reaction is not completed.

In order to evaluate the energy mixing in the intermediate complex, the average rotational and vibrational energies of the “old” fragment in reaction (c) were compared in Table III with those of the reactions (a) and (b),  $^{18}\text{O}(^1D) + N_2^{16}\text{O} \rightarrow N^{18}\text{O} + N^{16}\text{O}$  and  $^{16}\text{O}(^1D) + \text{H}_2^{18}\text{O} \rightarrow ^{16}\text{OH} + ^{18}\text{OH}$ . For the  $^{16}\text{O}(^1D) + \text{H}_2^{18}\text{O}$  reaction, several research groups have determined the products rotational and vibrational state distributions.<sup>15,16</sup> Since their data are similar, the latest one using the  $\text{O}_3$  photodissociation at 266 nm (Ref. 15) is listed in Table III. The available energies  $E_{\text{avail}}$  and the dissociation energies  $D_0$  of the intermediates which correspond to the well depths of PESs are also given in Table III. Since only the theoretical value of  $D_0$  from density functional theory calculations is available for SNNO to our best knowledge,<sup>5</sup>

TABLE III. Average rotational and vibrational energies of the “old” fragments for reactions (a), (b), and (c), together with the total available energies of the reactions and the binding energies of their intermediates ( $\text{cm}^{-1}$ ).

	$^{18}\text{O}(^1D) + \text{N}_2^{16}\text{O}$ $\rightarrow \text{N}^{18}\text{O} + \text{N}^{16}\text{O}$ [reaction (a)] <sup>a</sup>	$^{16}\text{O}(^1D) + \text{H}_2^{18}\text{O}$ $\rightarrow ^{16}\text{OH} + ^{18}\text{OH}$ [reaction (b)] <sup>b</sup>	$\text{S}(^1D) + \text{N}_2\text{O}$ $\rightarrow \text{NS} + \text{NO}$ [reaction (c)] <sup>c</sup>
$E_{\text{avail}}$	30000	11400	9400
$D_0$	700 <sup>d</sup>	17400 <sup>e</sup>	[ $\approx 700$ ] <sup>f</sup>
$\langle E_{\text{vib}} \rangle_{\text{expt}}$	$\approx 4000$ ( $\approx 0.63$ ) <sup>i</sup>	210 (0.16) <sup>i</sup>	550 (0.37) <sup>i</sup>
$\langle E_{\text{rot}} \rangle_{\text{expt}}$	[ $\approx 7000$ ] <sup>g</sup> [( $\approx 1.1$ )] <sup>i</sup>	1900 (0.68) <sup>i</sup>	1600 (0.84) <sup>i</sup>
$\langle E_{\text{vib}} \rangle_{\text{PST}}$	6400	1300	1500
$\langle E_{\text{rot}} \rangle_{\text{PST}}$	6400 <sup>h</sup>	2800	1900

<sup>a</sup>References 3 and 14.

<sup>b</sup>Reference 15.

<sup>c</sup>This work.

<sup>d</sup>Reference 4.

<sup>e</sup>Reference 11.

<sup>f</sup>This value is deduced from the results using DFT calculations of Ref. 5.

<sup>g</sup>This value is estimated from the rotational temperature of the  $\text{NO}(v=0)$  which obtained in the unlabeled experiments in Ref. 14.

<sup>h</sup>This value is evaluated from the prior distribution.

<sup>i</sup>Data given in parentheses are the ratios relative to the average energies predicted from phase space theory.

the binding energy of SNNO is estimated by using this value. The estimated energy size of SNNO is to be almost the same as that of  $(\text{NO})_2$ .

As Table III shows, the average vibrational energy  $\langle E_{\text{vib}} \rangle$  of reaction (a) is much larger than the other two reactions. Since the available energy is different among these three reactions, we have to compare the energy partitioning using the ratio of  $\langle E_{\text{vib}} \rangle$  to the value predicted from the PST. The order in the energy randomization thus estimated is reaction (a) > reaction (c) > reaction (b).

In the  $\text{S}(^1D) + \text{N}_2\text{O}$  reaction, the vibrational energy transferred to the old product amounts to 37% of the statistical prediction. Although the amount is approximately two-third of the reaction (a), it is more than twice of that in the reaction (b). This result shows that the energy mixing in the  $\text{S}(^1D) + \text{N}_2\text{O}$  reaction is definitely operative in spite of the shallow well of PES and the short lifetime of the intermediate, and confirms our conclusion in the previous paper<sup>3</sup> that the mass effect is more important than the well depth of the PES. The presence of light hydrogen atoms in reaction (b) significantly reduces the state density and the momentum coupling among the vibrational motion, resulting in the extremely inefficient energy partitioning in spite of the expected long lifetime.

#### IV. DISCUSSIONS

Since the lifetime is not the essential factor to control the energy partitioning in the reactions of our interest, we confine our discussion to other factors in vibrational energy mixing, the density of states and the coupling among the vibrational states. In the statistical limit, the rate of IVR is represented by Fermi's Golden Rule as<sup>17</sup>

$$k = \frac{2\pi v^2 \rho}{\hbar}, \quad (4)$$

where  $v^2$  is the square of effective coupling and  $\rho$  is the density of state. That is, the extent of energy randomization can be regarded to be proportional to the density of state and the square of effective coupling when the time for IVR is the same. These two universal factors are sensitive to the molecular properties such as the location and the masses of component atoms.

The heavy components within the intermediate complex usually generate low frequency vibrations to increase the density of state  $\rho$  and cause large momentum couplings among the vibrational modes to give large  $v^2$ .

#### A. Mass effect on the coupling parameter $v^2$

To discuss more quantitatively the mass effects on  $v^2$ , we adopt a model<sup>18</sup> whose Hamiltonian is represented by the zero-order and the coupling term as

$$H = H^0 + V. \quad (5)$$

For simplicity, we assume that (1) all zero-order vibrational states are regarded as local-mode harmonic oscillators and (2) a harmonic momentum coupling only contributes to the coupling between the harmonic oscillators. Then, the elements of Hamiltonian are

$$H^0 = \sum_i \left[ \frac{1}{2} G_{ii} p_i^2 + \frac{1}{2} k_{ii} q_i^2 \right], \quad (6)$$

$$V = \sum_{i \neq j} G_{ij} p_i p_j, \quad (7)$$

where  $p_i$ ,  $q_i$ ,  $k_{ii}$ , and  $G_{ij}$  denote the momentum, the displacement, the force constant of the  $i$ th oscillator, and the element of  $G$ -matrix,<sup>19</sup> respectively. In general, a potential coupling should also be considered as a harmonic coupling term of the Hamiltonian. However, for the systems with large momentum coupling, the potential coupling makes only a small contribution.<sup>18</sup> Under these assumptions, the only nonzero elements of Hamiltonian matrix corresponding to  $v$  are<sup>18</sup>

$$\begin{aligned} & \langle \dots, n_a, \dots, n_b, \dots | H | \dots, n_a, \dots, n_b, \dots \rangle \\ &= \sum_i \alpha_{ii} (2n_i + 1) = \sum_i \left( n_i + \frac{1}{2} \right) \hbar \omega_i, \\ & \langle \dots, n_a + 1, \dots, n_b - 1, \dots | H | \dots, n_a, \dots, n_b, \dots \rangle \\ &= -\alpha_{ab} [(n_a + 1)n_b]^{1/2}, \\ & \langle \dots, n_a - 1, \dots, n_b + 1, \dots | H | \dots, n_a, \dots, n_b, \dots \rangle \\ &= -\alpha_{ab} [n_a(n_b + 1)]^{1/2}, \\ & \langle \dots, n_a + 1, \dots, n_b + 1, \dots | H | \dots, n_a, \dots, n_b, \dots \rangle \\ &= \alpha_{ab} [(n_a + 1)(n_b + 1)]^{1/2}, \\ & \langle \dots, n_a - 1, \dots, n_b - 1, \dots | H | \dots, n_a, \dots, n_b, \dots \rangle \\ &= \alpha_{ab} [n_a n_b]^{1/2}, \end{aligned} \quad (8)$$

where  $n_i$  is the quantum number of the  $i$ th vibrational mode on the local-mode basis,  $\omega_i$  is the vibrational frequency, and  $\alpha_{ij}$  is the parameter of momentum coupling,

TABLE IV. The structures, local-mode vibrational frequencies, and relevant parameters of the reaction complexes used for the model calculations.

	$^{18}\text{ONN}^{16}\text{O}$ [reaction (a)]	$\text{H}^{16}\text{O}^{18}\text{OH}$ [reaction (b)]	SNNO [reaction (c)]
Structural parameters of A–B–C–D			
A–B length/Å	1.152 <sup>a</sup>	0.965 <sup>b</sup>	1.552 <sup>c</sup>
B–C length/Å	2.263 <sup>a</sup>	1.452 <sup>b</sup>	1.961 <sup>c</sup>
C–D length/Å	1.152 <sup>a</sup>	0.965 <sup>b</sup>	1.178 <sup>c</sup>
∠ABC angle/deg	97.2 <sup>a</sup>	100.0 <sup>b</sup>	135.4 <sup>c</sup>
∠BCD angle/deg	97.2 <sup>a</sup>	100.0 <sup>b</sup>	102.3 <sup>c</sup>
torsion/deg	0.0 <sup>a</sup>	112.0 <sup>b</sup>	0.0 <sup>c</sup>
Local-mode vibrational frequencies of A–B–C–D/cm <sup>-1</sup> <sup>d</sup>			
A–B stretch	1780 <sup>e</sup>	3610 <sup>f</sup>	1110 <sup>c</sup>
B–C stretch	135 <sup>e</sup>	847 <sup>f</sup>	151 <sup>c</sup>
C–D stretch	1830 <sup>e</sup>	3600 <sup>f</sup>	1770 <sup>c</sup>
∠ABC bend	325 <sup>e</sup>	1330 <sup>f</sup>	216 <sup>c</sup>
∠BCD bend	334 <sup>e</sup>	1330 <sup>f</sup>	314 <sup>c</sup>
torsion	117 <sup>e</sup>	313 <sup>f</sup>	594 <sup>c</sup>
$\Delta E_{\text{coll}}/\text{cm}^{-1}$	820 <sup>g</sup>	640 <sup>g</sup>	410 <sup>h</sup>
$\Sigma \alpha_{ij} ^2/\Sigma \alpha_{ii} ^2$	$4.9 \times 10^{-2}$	$5.2 \times 10^{-3}$	$6.3 \times 10^{-2}$

<sup>a</sup>Reference 20.<sup>b</sup>Reference 21.<sup>c</sup>This value is evaluated from the DFT calculations of Ref. 5.<sup>d</sup>These frequencies are calculated from the normal-mode vibrational frequencies.<sup>e</sup>Reference 22.<sup>f</sup>Reference 23.<sup>g</sup>Reference 24.<sup>h</sup>Reference 12.

$$\alpha_{ij} = \frac{G_{ij}}{2} \left[ \frac{\hbar \omega_i \hbar \omega_j}{G_{ii} G_{jj}} \right]^{1/2} \quad (9)$$

For the real systems, the coupling matrices are evaluated on the basis of the eigenvalues and eigenvectors for the most stable structure of the individual intermediates. The structural parameters for the intermediates of the three reactions and their local-mode frequencies are given in Table IV.<sup>5,12,20–24</sup> The sum of the squares of off-diagonal momentum coupling parameters relative to that of diagonal term is also given in the bottom row of the Table IV. This quantity approximately expresses the average strength of the coupling among the local-mode vibrations. Apparently, the hydrogen-containing intermediate  $\text{H}^{16}\text{O}^{18}\text{OH}$  gives the one-order of magnitude smaller value than the other intermediates, indicating a very small coupling among the local-mode vibrations. This trend originates from the small reduced mass in the local-mode vibration containing a hydrogen atom. Since  $G_{ii}$  is proportional to the inverse of the reduced mass of the local-mode, the hydrogen-containing local mode gives a large  $G_{ii}$  and hence a small  $\alpha_{ij}$ . In this manner, the presence of a light atom considerably reduce the momentum coupling and therefore reduces the rate of IVR. For the present four-atomic reactions,  $^{16}\text{O}(^1D) + \text{H}_2^{18}\text{O}$  shows a ten-times less efficient IVR compared with the  $^{18}\text{O}(^1D) + \text{N}_2^{16}\text{O}$  and  $\text{S}(^1D) + \text{N}_2\text{O}$  reactions.

## B. The state density at a relevant energy range

The reaction,  $\text{A} + \text{BCD}$ , is initiated by the collision of the atom A which has an intrinsic energy uncertainty of  $E_{\text{coll}}$  (Fig. 6). We assume that the intermediate complex in the

initial stage stores all the energy in the A–B local mode vibration. When the energy mixing (IVR) process proceeds from this state, we can roughly estimate the rate of IVR using Eq. (4) using the  $v^2$  and  $\rho$  which can be calculated from the model of the preceding section. Using the coupling-scheme given in the preceding section and the vibrational frequencies in Table IV, the densities of the zero-order vibrational states which can couple with the initial state, which is defined as  $\rho_{\text{direct}}$  in Fig. 6, are calculated. The resulting values for the reactions (a), (b), and (c) are  $0.0098/\text{cm}^{-1}$ ,  $0.0063/\text{cm}^{-1}$ , and  $0.0146/\text{cm}^{-1}$ , respectively. These values

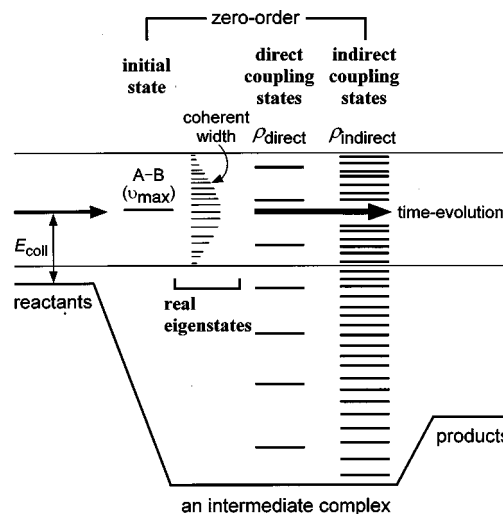


FIG. 6. A model for the time-evolution of IVR in an intermediate complex.

again suggest that the reaction (b) including light atoms has the small state density corresponding to 2/3 and 1/2 of the reactions (a) and (c).

The energy partitioning to the old NO is significantly larger while  $\rho_{\text{direct}}$  and  $v^2$  are smaller in the reaction (a) than in the reaction (c). This trend could be explained in terms of the background dark levels. The density of the background zero-order vibrational states ( $\rho_{\text{indirect}}$ ), which is not taken into account in the present coupling scheme, is much different between the reactions (a) and (c). Since the reaction (a) has a quite large exothermicity, the initially prepared intermediate contains a large amount of energy and the state density at this high energy level is quite large. Direct counting of the energy levels shows that  $\rho_{\text{indirect}}$ s are  $5.5 \times 10^4 \text{ cm}^{-1}$  for reaction (a) and  $1.1 \times 10^2 \text{ cm}^{-1}$  for reaction (c).

### C. The rate of IVR

To estimate the rate of IVR in the three relevant reactions, we use the analogy between the IVR in an intermediate complex and the time-evolution of the zero-order state which is prepared by an ultrashort coherent light pulse.

#### 1. Description of a model and the method of calculations

The IVR process can be considered as the evolution of an initial zero-order state  $|i\rangle$ , which is a superposition of many quantum eigenstates.<sup>25</sup> This initial zero-order state is, in general, prepared by an ultrashort pulse of light with wide energy range determined by the pulse duration. This ‘‘optical’’ initial state is not an eigenstate, but is represented by the superposition of eigenstates. The projection components of the dark zero-order states increase as the time-evolution of the initially prepared state. This process is the IVR in an ordinary rigid molecules excited by a fs light pulse.

In the present paper, this quantal scheme of IVR is adopted to interpret the energy randomization of the reaction intermediate, ABCD, generated from the bimolecular reaction, A+BCD. First, we assume that the initial zero-order state  $|i\rangle$  is the locally excited state, where only the A–B local-stretching vibration possesses all the available energy,  $E_{\text{avail}} + D_0$ , of the reaction. Because this reaction is initiated by the approach of the A atom to BCD, we regarded this as a suitable assumption. The initial state  $|i\rangle$  corresponds to a linear combination of many eigenstates  $|I\rangle$ ,

$$|i\rangle = \sum_I c_{Ii} |I\rangle. \quad (10)$$

The time evolution of this initial state is given by

$$\Psi(t) = \sum_I c_{Ii} |I\rangle \cdot e^{-iE_I t/\hbar}. \quad (11)$$

The dephasing of these eigenstates caused by their energy gaps leads to the increase of the projection components of the other local-mode vibrational states, i.e., the dark zero-order states. The energy randomization in the intermediate complex can be considered in this way as an IVR process similar to that in a stable molecule.

For the excitation by a laser pulse, the initial zero-order state is prepared by a quasi-delta-function pulse of light with

the energy of a finite width. In the present case of the bimolecular reaction, however, the initial state is produced by the collision between A and BCD. We assume that the coherent width of the initial state, which corresponds to the energy width of the ultrashort excitation pulse in the photoexcitation, can be defined as the collisional energy range of the incident atom. Since the reactant atom is generated by the photodissociation of O<sub>3</sub> or OCS, the collision energy of the atom has its intrinsic energy range. Although the distribution of this collision energy is not well-defined and the orientation of the collision is not fixed, the actual IVR can be interpreted as a superposition of the time evolution starting from a variety of coherently prepared initial state with a given coherent width. As a kind of thought experiment, we pursue the time evolution of such a coherent initial state and try to gain the information on the time scale of IVR in the particular reaction system.

Based on the above considerations, the loss of the initial zero-order state  $|i\rangle$  is obtained from the projection components of  $|i\rangle$  in the time-dependent wave function  $\Psi(t)$  as<sup>25</sup>

$$|\langle i|\Psi(t)\rangle|^2 = \left[ \sum_{I=1}^N |c_{Ii}|^4 + 2 \sum_{I>J} |c_{Ii}|^2 |c_{Ji}|^2 \cos \omega_{IJ} t \right], \quad (12)$$

where  $\omega_{IJ}$  is equal to  $(E_I - E_J)/\hbar$ . The fluorescence decay factor is omitted. The eigenvalues and the eigenvectors are obtained under the assumption of the local-mode description of the intermediate complex as given in the preceding section.

As is shown in Fig. 6 the initial zero-order states for <sup>18</sup>ONN <sup>16</sup>O [reaction (a)], H <sup>16</sup>O <sup>18</sup>OH [reaction (b)], and SNNO [reaction (c)] are considered as the local-mode vibrational states of the N–<sup>18</sup>O ( $v=17$ ), <sup>16</sup>O–H ( $v=8$ ), and N–S ( $v=8$ ) stretching modes, respectively. In this case, all eigenstates within the collision energy width  $\Delta E_{\text{coll}}$ , caused by the photodissociation of O<sub>3</sub> or OCS, are expected to contribute to the IVR. In the present calculations, the number of zero-order states were limited by truncating the interacting zero-order states according to the coupling strength. As the elements of basis set, we selected 162 zero-order states including one initial state, 26 states coupling with the initial state in the first-order perturbation level and 135 indirect-coupling states which become effective in the second-order perturbation level. With these 162 states, the eigenvectors and eigenvalues were computed by the matrix diagonalization. Then, the time evolutions of an initial state, the sum of direct-coupling states and the sum of indirect-coupling states were calculated for these three reaction intermediates.

### 2. Results of the model calculations

The time evolutions of the zero-order states in <sup>18</sup>ONN <sup>16</sup>O [reaction (a)] and H <sup>16</sup>O <sup>18</sup>OH [reaction (b)] are shown in Fig. 7. In the <sup>18</sup>ONN <sup>16</sup>O system [Fig. 7(a)], the population of the initial state decreases to 1/4 during the first 500 fs. At the same time, the other dark states rise with the same rate as the decline of the initial state. This means that the IVR in the intermediate <sup>18</sup>ONN <sup>16</sup>O proceeds in several

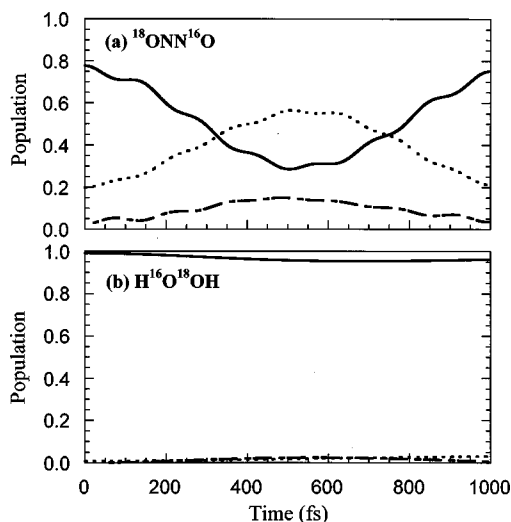


FIG. 7. Time profiles of the local-mode vibrational states in the reaction intermediates; (a)  $^{18}\text{ONN}^{16}\text{O}$  and (b)  $\text{H}^{16}\text{O}^{18}\text{OH}$ . The solid lines show the initial state populations, the dotted lines correspond with the sums of the direct-coupling states, and the dotted-and-dashed lines represent the sums of the populations of the indirect-coupling states.

hundred fs. If we take into account more background zero-order states in higher perturbation level, the population of the initial state should further decrease. The similar but slightly slower decay was observed for the SNNO system. The decay in the  $\text{H}^{16}\text{O}^{18}\text{OH}$  system [Fig. 7(b)] strongly contrasts with the  $^{18}\text{ONN}^{16}\text{O}$  case. In a period of 1 ps, the initial state decays by only 2%. Therefore, the available energy in the intermediate  $\text{H}^{16}\text{O}^{18}\text{OH}$  would not dissipate from the  $^{16}\text{O}-\text{H}$  local vibrational state to other degrees of freedom. Although the real decay of the initial local-mode vibration is expected to occur slightly faster than these calculations because of the participation of more zero-order states, we can roughly estimate the time required for the IVR from these simulations.

So far we mainly focus our attention on the magnitudes of  $v^2$  and  $\rho$ . However, the extent of IVR and hence the energy partition to the “old” product is also determined by another factor, the lifetime of the intermediate. Even though the IVR rate is slow, long lifetime could give a sufficient period for the IVR to complete. Therefore, we have estimated the lifetime of the intermediate and compared this figure with the IVR time obtained above.

The lifetime of the intermediate can be considered as the time during which the four atoms of the reaction system are interacting with each other. For the  $^{18}\text{O}(^1D) + \text{N}_2^{16}\text{O}$  reaction, we have estimated the lower limit of the interacting time. The velocity of  $^{18}\text{O}(^1D)$  generated from the  $^{18}\text{O}_3$  photolysis at 266 nm is  $\sim 2000 \text{ m s}^{-1}$ , corresponding to the velocity of about  $2 \text{ \AA}$  per 100 fs.<sup>24</sup> Since the average van der Waals radius of a  $\text{N}_2\text{O}$  molecule is  $4.9 \text{ \AA}$ , it takes 250 fs for an  $^{18}\text{O}(^1D)$  atom to pass the interaction region in a nonreactive encounter. Thus, 250 fs could be considered as the minimum “lifetime” of the intermediate. For the  $\text{S}(^1D) + \text{N}_2\text{O}$  reaction, such minimum lifetime would be longer because of the low velocity ( $\sim 1000 \text{ m s}^{-1}$ ) due to the heavy S atom.

From the model calculation of the  $^{18}\text{ONN}^{16}\text{O}$  interme-

diante, the population of the initial state is expected to decline to  $\sim 1/2$  during the interaction time of 250 fs estimated above. Therefore, it is likely that for the  $^{18}\text{O}(^1D) + \text{N}_2^{16}\text{O}$  reaction the necessary time for the IVR process is comparable to the minimum “lifetime” of the intermediate. We can conclude that IVR in the intermediate can proceed significantly even though the reaction is a direct process.

In the case of the  $^{16}\text{O}(^1D) + \text{H}_2^{18}\text{O}$  reaction with the deep well, the lifetime of the intermediate could be much longer than that of the  $^{18}\text{O}(^1D) + \text{N}_2^{16}\text{O}$  reaction. However, the IVR within the intermediate is quite slow as we showed in the preceding section. Using the molecular parameter given in Table IV, we have estimated the lifetime of the energized  $\text{H}^{16}\text{O}^{18}\text{OH}^*$  to be about 4 ps based on the RRK theory. Even within such a long lifetime, the IVR cannot proceed in the  $\text{H}^{16}\text{O}^{18}\text{OH}$  system because of the extremely slow IVR rate.

## V. SUMMARY AND CONCLUSIONS

We have determined the internal state distribution of “old”  $\text{NO}(X^2\Pi)$  generated from the reaction of  $\text{S}(^1D)$  with  $\text{N}_2\text{O}$ . The average vibrational energy of NO relative to the prediction by the statistical theory (PST) is found to be 37%. This figure suggests fairly effective energy randomization in the intermediate of the  $\text{S}(^1D) + \text{N}_2\text{O}$  reaction in spite of its short lifetime, and supports the previous conclusion for the  $^{18}\text{O}(^1D) + \text{N}_2^{16}\text{O}$  reaction.<sup>3</sup> The efficient IVR in the intermediate can be attributed to the presence of four heavy atoms in the system which provides low frequency vibrations to increase the state density and enhances the momentum coupling to facilitate the IVR.

A model calculation based on the local-mode vibrations with harmonic momentum coupling has been performed to estimate the mass effect on the state density and the momentum coupling. The coupling strength for the heavy atom system is found to be one-order of magnitude larger than that for the system containing hydrogen atoms. To estimate the rate of IVR, the quantal time evolution of the initial zero-order state has been calculated on the analogy of the coherent fs pulse excitation. The zero-order initial state is defined as the local-mode vibrational state where all available energy is accommodated in the stretching vibration of the new bond. The decay of such initial state takes about 250 fs for the  $^{18}\text{O}(^1D) + \text{N}_2^{16}\text{O}$  reaction, which is comparable to the estimated lifetime of the intermediate. We conclude from these calculations that the efficient energy randomization can occur even within a very short lifetime of the intermediate, if the reaction system is composed of heavy atoms. The mass effect on the momentum coupling and the state density plays a primary role in the energy partitioning.

## ACKNOWLEDGMENT

This work was supported in part by a Grant-in-Aid for Scientific Research on Priority Areas No. 07240102 from the Ministry of Education, Science, and Culture in Japan.

<sup>1</sup>R. D. Levine and R. B. Bernstein, *Molecular Reaction Dynamics and Chemical Reactivity* (Oxford University Press, New York, 1987).

<sup>2</sup>J. C. Polanyi, *Acc. Chem. Res.* **5**, 161 (1972).

- <sup>3</sup>H. Akagi, Y. Fujimura, and O. Kajimoto, *J. Chem. Soc., Faraday Trans.* **94**, 1575 (1998); *J. Chem. Phys.* (submitted).
- <sup>4</sup>M. P. Casassa, J. C. Stephenson, and D. S. King, *J. Chem. Phys.* **89**, 1966 (1988); J. R. Hetzler, M. P. Casassa, and D. S. King, *J. Phys. Chem.* **95**, 8086 (1991); B. J. Howard and A. R. W. McKellar, *Mol. Phys.* **78**, 55 (1993); A. Dkhissi, P. Soulard, A. Perrin, and N. Lacombe, *J. Mol. Spectrosc.* **183**, 12 (1997).
- <sup>5</sup>L. Andrews, P. Hassanzadeh, G. D. Brabson, A. Citra, and M. Neurock, *J. Phys. Chem.* **100**, 8273 (1996).
- <sup>6</sup>G. Black and L. E. Jusinski, *J. Chem. Phys.* **82**, 789 (1985).
- <sup>7</sup>W. H. Breckenridge and H. Taube, *J. Chem. Phys.* **53**, 1750 (1970); R. J. Donovan and W. H. Breckenridge, *Chem. Phys. Lett.* **11**, 520 (1971); G. Black, *J. Chem. Phys.* **84**, 1345 (1986).
- <sup>8</sup>M. W. Chase, Jr., C. A. Davies, J. R. Downey, Jr., D. J. Frurip, R. A. McDonald, and A. N. Syverud, *JANAF Thermochemical Tables*, 3rd Ed., *J. Phys. Chem. Ref. Data Suppl.* **14**, 1 (1985); *CRC Handbook of Chemistry and Physics*, 78th ed., edited by D. R. Lide (Chemical Rubber, Boca Raton, 1997).
- <sup>9</sup>N. van Veen, P. Brewer, P. Das, and R. Bersohn, *J. Chem. Phys.* **79**, 4295 (1983).
- <sup>10</sup>H. Okabe, *Photochemistry of Small Molecules* (Wiley, New York, 1978), pp. 237–244.
- <sup>11</sup>R. Atkinson, D. L. Baulch, R. A. Cox, R. F. Hampson, Jr., J. A. Kerr, and J. Troe, *J. Phys. Chem. Ref. Data* **21**, 1125 (1992).
- <sup>12</sup>N. Sivakumar, G. E. Hall, P. L. Houston, J. W. Hepburn, and I. Burak, *J. Chem. Phys.* **88**, 3692 (1988).
- <sup>13</sup>P. Pechukas and J. C. Light, *J. Chem. Phys.* **42**, 3281 (1965).
- <sup>14</sup>H. Tsurumaki, Y. Fujimura, and O. Kajimoto, *J. Chem. Phys.* (submitted).
- <sup>15</sup>D. G. Sauder, J. C. Stephenson, D. S. King, and M. P. Casassa, *J. Chem. Phys.* **97**, 952 (1992).
- <sup>16</sup>J. E. Butler, L. D. Talley, G. K. Smith, and M. C. Lin, *J. Chem. Phys.* **74**, 4501 (1981); K.-H. Gericke, F. J. Comes, and R. D. Levine, *ibid.* **74**, 6106 (1981); F. J. Comes, K.-H. Gericke, and J. Manz, *ibid.* **75**, 2853 (1981); C. B. Cleveland and J. R. Wiesenfeld, *ibid.* **96**, 248 (1992); N. Tanaka, M. Takayanagi, and I. Hanazaki, *Chem. Phys. Lett.* **254**, 40 (1996).
- <sup>17</sup>M. Bixon and J. Jortner, *J. Chem. Phys.* **48**, 715 (1968).
- <sup>18</sup>M. S. Child and R. T. Lawton, *Faraday Discuss. Chem. Soc.* **71**, 273 (1981); M. S. Child and L. Halonen, *Adv. Chem. Phys.* **57**, 1 (1984).
- <sup>19</sup>E. B. Wilson, Jr., J. C. Decius, and P. C. Cross, *Molecular Vibrations* (Dover, New York, 1980); J. C. Decius, *J. Chem. Phys.* **16**, 1025 (1948).
- <sup>20</sup>A. R. W. McKellar, J. K. G. Watson, and B. J. Howard, *Mol. Phys.* **86**, 273 (1995).
- <sup>21</sup>J. Koput, *Chem. Phys. Lett.* **236**, 516 (1995).
- <sup>22</sup>A. L. L. East, A. R. W. McKellar, and J. K. G. Watson, *J. Chem. Phys.* **109**, 4378 (1998).
- <sup>23</sup>P. A. Giguère and T. K. K. Srinivasan, *J. Raman Spectrosc.* **2**, 125 (1974); J. J. Hillman, D. E. Jennings, W. B. Olson, and A. Goldman, *J. Mol. Spectrosc.* **117**, 46 (1986); W. B. Olson, R. H. Hunt, B. W. Young, A. G. Maki, and J. W. Brault, *ibid.* **127**, 12 (1988); J.-M. Flaud, C. Camy-Peyret, J. W. C. Johns, and B. Carli, *J. Mol. Spectrosc.* **91**, 1504 (1989); C. Camy-Peyret, J.-M. Flaud, J. W. C. Johns, and M. Noël, *J. Mol. Spectrosc.* **155**, 84 (1992).
- <sup>24</sup>R. K. Sparks, L. R. Carlson, K. Shobatake, M. L. Kowalczyk, and Y. T. Lee, *J. Chem. Phys.* **72**, 1401 (1980).
- <sup>25</sup>P. M. Felker and A. H. Zewail, *J. Chem. Phys.* **82**, 2961 (1985); P. M. Felker and A. H. Zewail, in *Jet Spectroscopy and Molecular Dynamics*, edited by J. M. Hollas and D. Phillips (Blackie A&P, Glasgow, 1995), p. 222.